Chemistry Journals
Analytical, Inorganic, Organic, Physical, Materials Science

On the mechanism of automated fizzy extraction

Chun-Ming Chang [1,2], **Hao-Chun Yang** [1,2], **Pawel L Urban** [Corresp. 1,3]

[1] Department of Chemistry, National Tsing Hua University, Hsinchu, Taiwan

[2] Department of Applied Chemistry, National Chiao Tung University, Hsinchu, Taiwan

[3] Frontier Research Center on Fundamental and Applied Sciences of Matters, National Tsing Hua University, Hsinchu, Taiwan

Corresponding Author: Pawel L Urban
Email address: urban@mx.nthu.edu.tw

Fizzy extraction (FE) facilitates analysis of volatile solutes by promoting their transfer from the liquid to the gas phase. A carrier gas is dissolved in the sample under moderate pressure ($\Delta p \approx 150$ kPa), followed by an abrupt decompression, what leads to effervescence. The released gaseous analytes are directed to an on-line detector due to a small pressure difference. FE is advantageous in chemical analysis because the volatile species are released in a short time interval, allowing for pulsed injection, and leading to high signal-to-noise ratios. To shed light on the mechanism of FE, we have investigated various factors that could potentially contribute to the extraction efficiency, including: instrument-related factors, method-related factors, sample-related factors, and analyte-related factors. In particular, we have evaluated the properties of volatile solutes, which make them amenable to FE. The results suggest that the organic solutes may diffuse to the bubble lumen, especially in the presence of salt. The high signal intensities in FE coupled with mass spectrometry are partly due to the high sample introduction rate (upon decompression) to a mass-sensitive detector. However, the analytes with different properties (molecular weight, polarity) reveal distinct temporal profiles, pointing to the effect of bubble exposure to the sample matrix. A sufficient extraction time (~ 12 s) is required to extract less volatile solutes. The results presented in this report can help analysts to predict the occurrence of matrix effects when analyzing real samples. They also provide a basis for increasing extraction efficiency to detect low-abundance analytes.

On the mechanism of automated fizzy extraction

Chun-Ming Chang[1,2], Hao-Chun Yang[1,2], Pawel. L. Urban[1,3]

[1] Department of Chemistry, National Tsing Hua University, Hsinchu, Taiwan
[2] Department of Applied Chemistry, National Chiao Tung University, Hsinchu, Taiwan
[3] Frontier Research Center on Fundamental and Applied Sciences of Matters, National Tsing Hua University, Hsinchu, Taiwan

Corresponding Author:
Pawel L. Urban
Email address: urban@mx.nthu.edu.tw

Abstract

Fizzy extraction (FE) facilitates analysis of volatile solutes by promoting their transfer from the liquid to the gas phase. A carrier gas is dissolved in the sample under moderate pressure ($\Delta p \approx 150$ kPa), followed by an abrupt decompression, what leads to effervescence. The released gaseous analytes are directed to an on-line detector due to a small pressure difference. FE is advantageous in chemical analysis because the volatile species are released in a short time interval, allowing for pulsed injection, and leading to high signal-to-noise ratios. To shed light on the mechanism of FE, we have investigated various factors that could potentially contribute to the extraction efficiency, including: instrument-related factors, method-related factors, sample-related factors, and analyte-related factors. In particular, we have evaluated the properties of volatile solutes, which make them amenable to FE. The results suggest that the organic solutes may diffuse to the bubble lumen, especially in the presence of salt. The high signal intensities in FE coupled with mass spectrometry are partly due to the high sample introduction rate (upon decompression) to a mass-sensitive detector. However, the analytes with different properties (molecular weight, polarity) reveal distinct temporal profiles, pointing to the effect of bubble exposure to the sample matrix. A sufficient extraction time (~ 12 s) is required to extract less volatile solutes. The results presented in this report can help analysts to predict the occurrence of matrix effects when analyzing real samples. They also provide a basis for increasing extraction efficiency to detect low-abundance analytes.

Introduction

Sample preparation—whether performed in manual or automated manner—is frequently an unavoidable step in chemical analysis workflows (*Prabhu & Urban, 2017; Alexovič et al., 2018; Poole, 2020; Zheng, 2020*). It can rely on analyte transfer between different phases in liquid-liquid, solid-liquid, liquid-gas, or solid-gas extraction systems. One of the available approaches is the recently introduced fizzy extraction (FE) approach, which relies on dissolution of a carrier gas in

41   liquid sample under slightly elevated pressure, followed by a sudden decompression of the sample
42   headspace leading to effervescence (*Chang & Urban, 2016*; *Yang, Chang & Urban, 2017*).
43   Although the pressure applied to the sample is higher than the atmospheric pressure ($\Delta p \approx 150$
44   kPa), it is still very low in comparison with the pressures utilized in supercritical fluid methods
45   (~ 8-61 MPa) (*Hawthorne, 1990*). On decompression, multiple (micro)bubbles gush toward the
46   sample surface bringing analyte molecules to the gas phase. The effervescence in FE resembles
47   the phenomenon occurring in shaken soda bottle or in blood vessels of an individual suffering from
48   caisson disease. The surge of analyte molecules in the headspace (on the onset of effervescence)
49   gives rise to high transient analyte signals. FE may be regarded as a pressure-controlled
50   effervescence-assisted emulsification liquid-gas extraction approach.

51   FE was originally coupled with atmospheric pressure chemical ionization (APCI) mass
52   spectrometry (MS), which enabled real-time monitoring of the released medium-polarity volatile
53   and semivolatile compounds (*Chang & Urban, 2016*). Chemical analysis by FE hyphenated with
54   APCI-MS provides satisfactory detectability because the volatile organic compounds (VOCs) are
55   liberated and reach the ion source of mass spectrometer in a short period of time (few seconds).
56   The entire workflow is expeditious (< 5 min). Recently, FE was also hyphenated with gas
57   chromatography (*Yang & Urban, 2019*), and the extraction procedure was supplemented with
58   automated features (*Yang, Chang & Urban, 2019*). Partial automation is critical for repetitive
59   control of the saturation and effervescence steps. Although the FE system has not yet been
60   commercialized, it can readily be built by chemists using inexpensive modules (*cf. Urban, 2018*).

61   The earlier work on FE raised questions about the possible mechanism responsible for the
62   release of molecules into the gas phase. With the lack of a plausible description of the underlying
63   principles, it is unclear in which cases the procedure can be applied and how to boost its
64   performance. Therefore, in the present study, we attack the problem of FE mechanism. For that
65   purpose, we first identify a number of factors that can potentially influence FE performance.

66

Materials & Methods

68

Materials and samples

70   Ethanol (anhydrous, 99.5+%) was from Echo Chemical (Miaoli, Taiwan). Ethyl propionate (EPR),
71   ethyl pentanoate (EPE), ethyl hexanoate (EHX), ethyl nonanoate (EN), ethyl undecanoate (EUD),
72   and polyethylene glycol (PEG) 400 were from Alfa Aesar (Ward Hill, MA, USA). Ethyl butyrate
73   (EB) was from Acros Organics (Pittsburgh, PA, USA). Ethyl heptanoate (EHP) was from TCI
74   (Tokyo, Japan). Ethyl octanoate (EO), ethyl decanoate (ED), gum arabic (GA, from acacia tree),
75   and (R)-(+)-limonene (LIM) were from Sigma-Aldrich/Merck (St. Louis, MO, USA). 2-Propanol
76   (Emsure ACS, ISO, Reag. Ph Eur grade), methanol (LC-MS-grade), and water (LC-MS-grade)
77   were from Merck (Darmstadt, Germany). Sodium chloride was from Showa Chemical (Tokyo,
78   Japan). Sodium dodecyl sulfate (SDS; >90%) was from Aencore Chemical (Melbourne, Australia).
79   Typically, the stock solutions of chemical standards were prepared in pure alcohols (methanol,
80   ethanol, and isopropanol). The stock solution concentration (EPR, EPE, EHP, EN, EUD, and LIM)

81 was 1 M. The test samples containing ethyl esters with various carbon chains and LIM were
82 prepared in alcohol/water mixture at varied percentage (depending on the experiments). The final
83 concentration of chemical standards in the samples used in most experiments was 5×10^{-6} M.
84

Apparatus

86 The extraction process is facilitated by two microcontrollers (chipKIT Uno32 and Arduino Mega
87 2560), which are programmed in C++. The program-controlled pressure changes lead to repeatable
88 bubbling in the extraction chamber. The system also features a number of functions, which reduce
89 human effort. Some of these functions are utilized in the present study (controlling valves and
90 motor at defined time points, displaying experimental conditions on an LCD screen, and triggering
91 MS data acquisition). V1 (solenoid valve) is used to control the flow of the carrier gas (typically,
92 carbon dioxide), and it is connected to the sample chamber (20 mL screw top headspace glass vial
93 with septum cap; cat. no. 20-HSVST201-CP; Thermo Fisher Scientific, Waltham, MA, USA) *via*
94 a 20-cm section of polytetrafluoroethylene (PTFE) tubing (I.D. = 0.8 mm, O.D. = 1.6 mm, cat. no.
95 58700-U, Supelco; Sigma-Aldrich). A 14-cm section of soft rubber-like tubing (*e.g.* silicone
96 tubing, I.D. = 0.9 mm, O.D. = 2.0 mm) is attached to V2 (pinch valve), and it is connected in
97 between a 2-cm section of PTFE tubing (I.D. = 0.3 mm, O.D. = 1.6 mm, cat. no. 58702, Supelco;
98 Sigma-Aldrich) and a 60-cm section of ethylene tetrafluoroethylene (ETFE) extract transfer tubing
99 (I.D. = 1.0 mm, O.D. = 1.6 mm, part no. 1517L; IDEX Health & Science, Lake Forest, IL, USA).
100 During the optimization of extract transfer tubing diameter, various PTFE tubings (I.D. = 0.3 mm,
101 O.D. = 1.6 mm, cat. no. 58702; I.D. = 0.6 mm, O.D. = 1.6 mm, cat. no. 58701; I.D. = 0.8 mm,
102 O.D. = 1.6 mm, cat. no. 58700-U; Supelco; Sigma-Aldrich as well as I.D. = 1.0 mm, O.D. = 1.5
103 mm, from an unspecified supplier) were used instead of the ETFE tubing. The gaseous extract is
104 transferred from the extraction chamber via those tubing sections (PTFE, soft rubber-like, and
105 ETFE) to the ion source of mass spectrometer.
106

Procedure

108 An automated FE system was disclosed earlier (*Yang, Chang & Urban, 2019*), and it was applied
109 in this study following some modifications (*e.g.* removing T-junction and Valve 3, thermal printer,
110 wireless control, and real-time data processing) (**Fig. 1**). The FE process consists of three steps
111 (*Chang & Urban, 2016*):
112 I. Flushing step: Flushing headspace vapors with carrier gas (typically, carbon dioxide)
113   (60 s) (open Valves 1 and 2 (V1 and V2)).
114 II. Saturation step: Pressurizing carrier gas in the extraction chamber (open V1, and close
115   V2). Stirring is applied in this step to assist the dissolution of the carrier gas in the
116   sample matrix (60 s).
117 III. Extraction step: Depressurizing the sample chamber and transferring the gaseous
118   extract to APCI-MS. In the *stage 1* of this step (close V1, and open V2), the dissolved
119   carrier gas is released from the sample matrix, leading to effervescence. The VOCs are
120   extracted during this short period of time (2 s), and transferred to APCI-MS (see

121   Supporting Information text and **Table S1**). In the *stage 2* of this step (open V1 and

122   V2), the carrier gas flow is switched on again to assist in the transfer of the remaining

123   gas-phase analytes present in the sample headspace (28 s).

124 The default conditions used in most experiments are as follows: sample, 5×10^{-6} M analytes

125 dissolved in 5 vol. % of alcohol/water mixture; carrier gas, carbon dioxide; extract transfer tubing,

126 I.D. = 1.0 mm; extract transfer tubing length, 60 cm.

127

128 **Mass spectrometry**

129 Unless noted otherwise, the sample chamber was coupled *via* V2 and 60-cm (ETFE) extract

130 transfer tubing with triple quadrupole mass spectrometer (LCMS-8030; Shimadzu, Tokyo, Japan).

131 It was used in conjunction with DUIS ion source (Shimadzu) operated in the APCI positive-ion

132 mode. The potential applied to the APCI needle was 4.5 kV. Nebulizer gas (nitrogen) flow rate

133 was 2.5 L min^{-1}. Drying gas (nitrogen) flow rate was 15 L min^{-1}. The temperature of the desolvation

134 line was set to 250 °C, while the temperature of the heated block was set to 300 °C. The data

135 acquisition was performed in multiple reaction monitoring (MRM) mode (see **Table S1** for

136 transitions). The pressure of the collision gas (argon) was set to 230 kPa. The dwell time was 100

137 ms.

138

139 **Data treatment**

140 Enhancement factor (EF) is defined as the maximal signal intensity ($I_{\text{max-extraction}}$) in the extraction

141 step divided by the mean signal intensity ($mean_{\text{flushing}}$) during the flushing step (from 0.49 to 1.00

142 min):

143   $\text{EF} = \dfrac{I_{\text{max}-\text{extraction}}}{mean_{\text{flushing}}}.$ (1)

144 Signal-to-noise ratio (S/N) was calculated using the maximal signal intensity in the extraction step

145 minus the average intensity of the saturation step (local baseline, from 1.35 to 1.85 min) divided

146 by the root mean square of the blank sample in the extraction step (from 2.04 to 2.97 min):

147   $S/N = \dfrac{(I_{\text{max}-\text{extraction}} - mean_{\text{flushing}})}{RMS_{\text{extraction (blank)}}}.$ (2)

148 In one part of this study—in order to compensate for differences in ionization efficiencies of the

149 tested analytes—the corrected signal ($S_{\text{corrected}}$) was calculated based on the maximal signal

150 intensity obtained in FE ($I_{\text{max-FE}}$) multiplied by a correction factor:

151   $S_{\text{corrected}} = I_{\text{max}-\text{FE}} \times \text{CF}.$ (3)

152 The correction factor (CF) is defined as the average (averaging interval: 1 min) extracted ion

153 currents (EICs) of the target analytes (I_{target}) obtained in direct liquid infusion to APCI-MS (sample

154 flow rate, 40 µL min^{-1}; sample, 5×10^{-6} M analytes dissolved in 5 vol. % ethanol/water mixture)

155 divided by the average intensity of EPR (I_{EPR}, used as a reference; averaging interval: 1 min):

156   $\text{CF} = \dfrac{I_{\text{target}}}{I_{\text{EPR}}}.$ (4)

157 The calculations were done using Excel (version 16.0; Microsoft, Redmond, WA, USA) and
158 Matlab software (version R2017a; MathWorks, Natick, MA, USA). Origin software (version
159 2018b; OriginLab, Northampton, MA, USA) was used to plot the figures.
160

Results

162 To shed light on the mechanism of FE, we have studied the influence of a number of parameters
163 on the extraction process. These parameters are grouped into four categories: (1) instrument-
164 related; (2) method-related; (3) sample-related; (4) analyte-related.
165

Instrument-related factors affecting FE

Extract transfer tubing diameter and length

168 First, we tested 30-cm sections of four types of polytetrafluoroethylene (PTFE) tubing with
169 different inner diameters (0.3, 0.6, 0.8, and 1.0 mm) as extract transfer tubing. The EFs and *S/N*
170 increased as the inner diameter increased, especially for EPE, EHP, EN and LIM (**Fig. 2A**). More
171 gas-phase analyte molecules could be transferred to the MS ion source per time unit when a tubing
172 with a larger diameter was used. We further verified the influence of the extract transfer tubing
173 length (30, 40, 50, 60 cm; I.D. = 1.0 mm) on the extraction process. The EFs and *S/N* of medium-
174 volatility compounds (EPE, EHP, and LIM) increased with the increasing tubing length (**Fig. 2B**).
175 This result may be related to the fact that the use of longer tubing leads to a lower gas flow rate
176 (*Coelho & Pinho, 2007*).
177

Method-related factors affecting FE

Gas type

180 It is known that different gases form bubbles with different size (*Hanafizadeh et al., 2015*). While
181 carbon dioxide is mainly used to produce fizzy drinks, nitrogen is occasionally used (*Hildebrand*
182 *& Carey, 1969*). Here, five easily available gases (carbon dioxide, nitrogen, air, argon, and
183 helium), with different physical properties, were investigated. Based on the recorded EFs and *S/N*,
184 all the tested gases can be used in FE (**Fig. 3A**). However, extraction of one compound (EPE) was
185 clearly affected by the type of gas used. In the case of carbon dioxide, the EF was the lowest, while
186 in the case of helium, it was the highest. According to Eq. (1), high EF can be either due to high
187 amplitude of signal in extraction step or low amplitude of signal in flushing step. Solubility of
188 gases in water (*Gevantman, 2000*) can influence the dissolution of gases during pressurization,
189 thus affecting the formation of bubbles. Moreover, the densities of the tested gases are dissimilar
190 (*Rathakrishnan, 2004*). These different densities can also contribute to some selectivity in VOC
191 removal from the sample headspace in the flushing step. Owing to the poor solubility of helium in
192 water, and its low density, helium may predominantly flow in the upper part of the headspace in
193 the sample chamber, scavenging highly volatile analytes, which easily diffuse to the upper section
194 of the sample chamber. Therefore, the signals of VOCs during headspace flushing are generally
195 low when using helium as carrier gas (**Fig. S1**).
196

Fast decompression vs. slow decompression

197 *Fast decompression vs. slow decompression*
198 The rationale of this test builds on a daily-life observation: When one slightly loosens cap of a
199 carbonated drink bottle, numerous microbubbles or foam are formed. Conversely, when one
200 unscrews the cap rapidly, the emerging bubbles quickly coalesce, leading to a smaller number of
201 large bubbles. Microbubbles have higher surface area-to-volume ratio than large bubbles
202 (*Zimmerman et al., 2008*). Thus, liquid-gas phase equilibrium should be established in
203 microbubbles faster than in large bubbles.
204 To emulate the process of slow decompression, we pulsed V2 with different open duty cycles
205 while the cycle duration was fixed at 400 ms. At first, we only applied pulsations in the *stage 1* of
206 the extraction step (for 2 s). For all the tested conditions, the results did not show clear trends (**Fig.
207 3B**), and the temporal profiles recorded in different variants of decompression were similar (**Fig.
208 S2**). In order to verify the effect of slow decompression on FE, we further applied pulsations not
209 only in the *stage* 1 but also in the *stage 2* of the extraction step (for 30 s). Although no obvious
210 changes were observed, EN exhibited a slightly higher EF and *S/N* with 25% open duty cycle than
211 in other conditions (**Fig. 3C**). Moreover, the tested analytes revealed distinct temporal profiles
212 when open duty cycles were varied (**Fig. S3**). The areas under the curve (ion current of the
213 extraction step) increased with decreasing open duty cycles (**Fig. S4**). This observation shows that,
214 when the gaseous extract is transferred to MS in pulses (rather than continuously), the sample can
215 still be extracted continuously providing high VOC signals.
216 We also conducted an experiment, in which we changed the duration of the *stage 1* of the
217 extraction step. The EFs and *S/N* ratios were not affected to a great extent in most of the tested
218 compounds except EHP (**Fig. 3D**). The decline in EF of EHP with increasing extraction time may
219 be because the extracted EHP molecules were not concentrated in the headspace of the sample
220 chamber sufficiently, and were transferred to the detector at different time points leading to two
221 temporal peaks (**Fig. S5**, extraction time, 10 s). The appearance of the first peak is linked to the
222 VOCs that were extracted during effervescence (*stage 1*), while the second peak is linked to the
223 scavenging of the headspace vapors by pumping the carrier gas (*stage 2*). The observation that the
224 second peak was higher than the first peak (EHP and EN, 10 s) could be explained in the following
225 way: The amount of dissolved carbon dioxide was insufficient to extract and scavenge the analytes
226 with higher molecular weights and lower polarities in the *stage 1*. Scavenging of these analytes
227 continued after opening V1.
228
229 **Sample-related factors affecting FE**
230 *Sample solvent*
231 **Figures 4A-4C** show the influence of organic solvents—present in the sample—on the extraction
232 efficiency. Notably, the EFs and *S/N* decreased with increasing ethanol concentration. This effect
233 is rationalized in the following way: Medium and low-polarity VOCs partition to the liquid phase
234 because of their good solubility in ethanol. Moreover, the surface tension of sample matrix
235 decreases with increasing ethanol concentration, which results in larger bubble size (**Fig. S6C**).
236 Overall, FE can be performed on samples containing common alcohols in a broad concentration

237 range (0.1-25 vol. %). The three tested alcohols provide similar extraction performances. However,
238 ethanol is the solvent of choice due to its lower toxicity. In addition, ethanol is present in alcoholic
239 beverages, which can readily be analyzed by FE. In this case, the sample pretreatment can be
240 reduced to simple dilution with pure water.
241

242 *Presence of salt*
243 Addition of an electrolyte into an aqueous solution can affect partitioning of the organic solutes
244 between the liquid phase and gas phase. Here, we investigated the effect of NaCl at varied
245 concentrations on extraction efficiency of the test analytes. Although the EF of the chosen
246 compounds did not reveal major differences, the *S/N* showed clear ascending trends for the
247 increasing concentrations of NaCl, especially for the highly volatile compounds (EPR, EPE, EHP;
248 **Fig. 4D**). This result can be explained with the occurrence of 'salting out effect' (see below) (*Hyde*
249 *et al., 2017*).
250

251 *Presence of surfactants and related additives*
252 It is known that surface-active agents (so-called 'surfactants') can drastically influence bubble
253 behavior; reduce rising velocity, prevent coalescence, and deplete/enhance mass transfer (*Takagi*
254 *& Matsumoto, 2011*). Here, we evaluated the effect of two commonly used surfactants (GA and
255 SDS)—at concentrations below the critical micelle concentrations (*Moroi, Motomura & Matuura,*
256 *1974*)—on the extraction of the target analytes. As expected, the foam height increased notably
257 with the increasing concentration of GA (**Fig. S6C**). This phenomenon can be explained with the
258 reduction of solution surface tension by GA, which promotes liberation of the dissolved gas (*Cao*
259 *et al., 2013*), and stabilization of the interfacial film (*Wyasu & Okereke, 2012*). Nonetheless, we
260 only observed a slight increase of EF and *S/N* in LIM (**Fig. 4E**). Similar to GA, the foaming height
261 increases in the presence of SDS (**Fig. S6C**), an anionic surfactant. The EF and *S/N* of medium
262 polarity compounds (EHP, EN, LIM) revealed a slightly ascending trend for increasing
263 concentrations of SDS (**Fig. 4F**).
264   Because interfacial rheological properties can greatly alter bubble stability by affecting the mass
265 transfer across the interface (*Pelipenko et al., 2012*), we took advantage of the strongly hydrophilic
266 and viscous nature of PEG400 (a surfactant-related additive) (*Harris, 2013*) to evaluate its effect
267 on the extraction performance of the selected analytes. The foaming height of the PEG400-
268 containing sample was greater than the one without adding PEG400 (**Fig. S6C**). However, only
269 the EF and *S/N* ratios of two compounds (EHP, LIM) were slightly increased when the
270 concentration of PEG400 was increased (**Fig. 4G**).
271

272 *Presence of gas bubble nucleation sites*
273 One technology used by beer industry to control bubbling involves coating the inner walls of
274 bottles with cellulose fibers to increase the abundance of nucleation sites (*Liger-Belair, Polidori*
275 *& Jeandet, 2008*; *Lee & Devereux, 2011*). Formation of nucleation sites in carbonated liquids with
276 low supersaturation ratios (*e.g.* carbonated beverages, sparkling wines) requires the presence of

277   gas pockets with radii of curvature larger than the critical nucleation radius (typically, < 1 µm)
278   (*Jones, Evans & Galvin, 1999*; *Liger-Belair, 2005*). At this condition, the nucleation energy barrier
279   is overcome, thus promoting bubble growth (type IV non-classical nucleation, according to the
280   nomenclature by Jones *et al.*). (*Jones, Evans & Galvin, 1999*; *Lubetkin, 2003*) The tiny and hollow
281   cavities within cellulose fibers (lumens) are responsible for the production of bubble trains, and
282   are regarded as one of the most abundant sources of nucleation sites (*Liger-Belair, Voisin &*
283   *Jeandet, 2005*). Therefore, we intentionally introduced different numbers of cotton fibers to the
284   sample chamber to increase the abundance of nucleation sites. Although no obvious differences in
285   EFs were observed, a slight increase of *S/N* ratios could be seen (**Fig. 4H**).

286

287   **Analyte-related factors affecting FE**
288   *Analyte properties*
289   To characterize general applicability of FE, we tested a series of ethyl esters with different carbon
290   numbers (C_5-C_{13}) as model analytes (**Table S2**). The dependencies of EFs and *S/N* ratios on the
291   investigated physical properties showed distinct trends revealing the amenability of most of the
292   tested compounds to analysis by FE-APCI-QqQ-MS (**Fig. 5**). This result is in line with the result
293   obtained by FE-GC-Q-MS (*Yang & Urban, 2019*).
294   In the case of the highly volatile compounds (*e.g.* EPR, EB), the intensities of EICs in the
295   flushing and extraction steps are similar, resulting in low EFs. This observation is explained with
296   the fact that the liquid-gas equilibrium is established rapidly. In addition, these polar short-chain
297   ethyl esters strongly interact with solvent molecules, thus limiting their transfer to the gas phase
298   (bubble, headspace) during effervescence. On the other hand, in the case of less volatile
299   compounds (*e.g.* ED, EUD), the poor EFs may be attributed to their low vapor pressures and high
300   molecular weights. Since the mass transfer of big molecules into the bubbles (predominantly by
301   diffusion) is limited, only a small portion of these low-volatility species can be transferred to the
302   gas phase, leading to low MS signal intensities.
303   Ionization efficiencies may differ for the tested analytes, possibly leading to misinterpretation
304   of the results. To compensate for the anticipated ionization bias, we applied correction factors (see
305   Eq. (3)) obtained by direct liquid infusion to the FE results. Overall, the analytes characterized
306   with satisfactory EFs, *S/N*, and corrected signal intensities are those that contain 7-10 carbon
307   atoms, have boiling points in the range of 420-480 K, logarithm of octanol-water partition
308   coefficient values in the range of 1.8-3.3, surface tensions in the range of 0.0265-0.0285 N m^{-1},
309   vapor pressure values in the range of 0.03-0.63 kPa, and solubilities in water in the range of 0.08-
310   3.71 g kg^{-1} (**Fig. 5**). They are highly amenable to FE (EFs ranging from 15 to 75).

311

312   **Note on the data variability**
313   To verify the reliability of the results obtained in this study, we further evaluated the
314   reproducibility of the FE technique at the default conditions (carrier gas, carbon dioxide; extract
315   transfer tubing, I.D. = 1.0 mm; extract transfer tubing length, 60 cm; solvent, 5 vol. % ethanol in
316   water). In the case of EFs, the dense distribution of the data points implies good reproducibility

317 among numerous replicates ($n = 33$; 11 days; **Fig. S7**). However, in the case of *S/N*, the data cloud
318 shows a broader distribution, especially for EPR, EPE, and EHP (**Fig. S7**). This can be rationalized
319 with the technical variability of the instrument conditions, which may contribute to different MS
320 signal intensities and spectral noise on different days. It is evident that using EFs is a proper way
321 to evaluate extraction performance of FE. By calculating EFs, one can quantify the differences
322 between FE and direct headspace vapor flushing in a single experiment. The use of EFs ensures
323 satisfactory (inter-day) reproducibility, mitigates the effect experimental variability, which would
324 otherwise obscure relevant trends.

325

Discussion

327 It was earlier demonstrated that removal of VOCs from aqueous samples can be greatly enhanced
328 with the aid of microbubbles generated by purging such samples with gases delivered to the bottom
329 of the sample vessel (*Wang & Lenahan, 1984*; *Shimoda et al., 1994*). However, the use of relatively
330 long sample column and large sample volumes are critical to achieve satisfactory extraction
331 efficiencies. To boost analytical performance, the effluent gas extracts are often trapped prior to
332 analysis, as it is in purge-closed-loop and purge-and-trap methods (*Wang & Lenahan, 1984*; *Abeel,*
333 *Vickers & Decker, 1994*). In general, the gas stripping approach—relying on concentration of the
334 liberated analytes into small volumes—is time-consuming, requires the supply of energy
335 (electricity for heating) and additional consumable materials (sorbent, cryogenic agent).
336   In FE—unlike in the sparging techniques—numerous microbubbles are formed *in situ* during
337 fast decompression (**Fig. 6**). These microbubbles further grow due to absorption of dissolved gas
338 (*Fang et al., 2016*), and coalesce with other (micro)bubbles (*Chaudhari & Hofmann, 1994*).
339 Previously, we showed that increasing carbon dioxide pressure (0-150 kPa) during saturation leads
340 to increased analyte peak areas during FE (*Chang & Urban, 2016*). This effect can be attributed
341 to the greater number of microbubbles formed when the concentration of the dissolved gas is
342 higher. However, due to practical and safety-related issues, we did not further utilize higher
343 pressures than 150 kPa. The addition of surfactant can reduce the surface tension, and alter the
344 viscosity of the solution, thus increasing the number of microbubbles. However, the use of
345 surfactants may also cause unmanageable foaming problems leading to contamination of flow lines
346 with sample droplets and foam. In fact, the foaming height increased notably in the presence of
347 surfactant-related additives (**Fig. S6C**). Thus, in order to prevent contamination of the system, the
348 concentration of surfactants cannot be too high. Only few compounds (EHP, LIM) showed slightly
349 higher EFs and *S/N* when the surfactant concentration was increased (**Fig. 4E-4G**). Accordingly,
350 one does not anticipate major matrix effects at low concentrations of surfactants present in the
351 analyzed samples.
352   Microbubbles can readily form at nucleation sites (*e.g.* rough surface, lumen of cellulose fibers)
353 (*Jones, Evans & Galvin, 1999*). Thus, in one experiment, we introduced cotton fibers into the
354 sample chamber to provide nucleation sites. The fact that the improvement of FE performance was
355 only minor (**Fig. 4H**) could be due to an uneven distribution of cotton fibers or insufficient number
356 of microbubbles generated with the aid of the air trapped within fiber lumens. It should be noted

357 that the air entrapment is attributed to the fact that the time required for the liquid to fully invade
358 the lumen by capillary action is longer than the time required to submerge the fibers (*Liger-Belair,*
359 *2012*). However, mechanical stirring—applied in the *stage 2* of the extraction step—can enhance
360 contact between fiber lumens and solvent, thus eliminating the trapped air and reducing the
361 formation of microbubbles. On the other hand, stirring itself can promote formation of bubbles
362 (*Dean, 1944*).
363   FE showed poor performance at the high concentrations (> 25 vol. %) of alcohols (**Fig. 4A-C**).
364 This result is explained with an elevated partitioning of organic solutes to the liquid phase. In
365 addition—according to the Stokes' equation (*Stokes, 1851*)—when the bubble size becomes large,
366 the rise rate of such bubbles increases:

367 $$R = \frac{\rho g D^2}{18\mu},$$ (5)

368 where R is bubble rise rate (m s^{-1}), ρ is density (kg m^{-3}), D is diameter (m), and μ is dynamic
369 viscosity (kg m^{-1} s^{-1}). High rise rates increase the probability of bubble coalescence, thus reducing
370 bubble density (*Rajib, Farzeen, & Ali, 2017*). The observed reduction of bubbling and large bubble
371 size at high alcohol concentration (**Fig. S6C**) can also be attributed to the decreased surface tension
372 (*Rajib, Farzeen, & Ali, 2017*). Down this path, few large bubbles provide smaller liquid-gas
373 interface surface area than many microbubbles, while high rise rate shortens the time of their
374 exposure to the sample, what—along the increased partitioning to the liquid phase—leads to low
375 extraction yields.
376   Enrichment of organic solutes by 'bursting bubble aerosols' is based on the assumption that
377 analyte molecules can adsorb on bubble surface during its exposure to sample matrix, and then are
378 released to the headspace via microdroplets ejected from the bubble surface (*Chingin et al., 2016*;
379 *Chingin et al., 2018*). The number of adsorbed molecules can gradually increase as bubbles grow.
380 Moreover, other solutes can expel some of the analytes from the liquid phase, contributing to
381 adsorption of these analytes onto bubble surface. The so-called 'salting effect' is described by
382 Setschenow equation (*Setschenow, 1889*):

383 $$log\frac{S}{S_o} = -K_{salt}C_{salt},$$ (6)

384 where S is the solubility of the organic solute in aqueous solution, S_o is the solubility of the organic
385 solute in pure water, K_{salt} is the empirical Setschenow constant, and C_{salt} is the molar concentration
386 of the electrolyte. As the concentration of salt increases, the solubility of the organic solutes in the
387 salt solution decreases due to the electrostatic interactions between the salt ions and water dipoles,
388 which reduce the number of freely available water molecules in the solution (*Hyde et al., 2017*).
389 Hydrophobic interactions are promoted leading to aggregation of the organic solutes (*Thomas &*
390 *Elcock, 2007*). Therefore, the organic species distribute near the liquid-air interface, and are
391 concentrated in the headspace by the bursting bubbles. In the case of highly volatile and polar
392 compounds, a notable increase in *S/N* ratios but no major differences in EFs were observed in the
393 presence of salt (**Fig. 4D**). However, no clear trend was observed for the less volatile and less polar
394 compounds. These results suggest that—when a bubble rises up—it preferentially scavenges low-
395 molecular-weight (here, polar) compounds. An adsorption equilibrium at the bubble surface may

396 be established rapidly when large quantities of low-molecular-weight polar compounds are present
397 near the interface, and only limited space is available for non-polar solutes (with higher molecular
398 weight) to adsorb. Insufficient adsorption space at the bubble surface may be responsible for poor
399 extraction efficiency of less volatile compounds in FE.
400 The type of carrier gas only had a minor effect on FE. The solubility of the gas greatly influences
401 the amount of bubbles produced during effervescence. Therefore, different MS ion signal
402 intensities are recorded in the extraction step when different gases are used (**Fig. S1**). Moreover,
403 the five tested gases have non-polar character. Other available gases (*e.g.* with higher polarity)
404 were not considered mainly due to safety reasons. It is imaginable that compounds with non-polar
405 moieties may adsorb on the bubble surface. However, the signals of low-polarity compounds were
406 lower than those of medium-polarity compounds (**Fig. 5C**).
407 It is also imaginable that the low-molecular-weight (volatile) molecules diffuse into the bubble
408 lumen, or are incorporated into the bubble during bubble growth ("co-precipitation" into the gas
409 phase). Since the applied gases are non-polar, the lower-polarity analytes should, in principle, be
410 preferentially extracted by the bubbles, entering their lumens. However, against intuition, the
411 lowest polarity compounds in the tested set do not show the highest EFs, *S/N*, and corrected signal
412 intensities (**Fig. 5C**). Furthermore, the diffusion coefficients of the solutes in the solvent and across
413 the solvent-gas interface can alter their transfer to the bubble surface and across the interface. Note
414 that the diffusion coefficients of gases are related to their molecular weight (*Mason & Kronstadt,*
415 *1967*). Turbulence—due to stirring and effervescence—can improve the mass transfer
416 (*Sandoval-Robles, Delmas & Couderc, 1981*) of solutes to the proximity of liquid-gas interface
417 (bubbles, headspace) but it may not necessarily affect the mass transfer across the liquid-gas
418 boundary around the bubbles. When salt is present in the sample, the organic solutes may partition
419 into this boundary. However, the extraction of the lower-polarity analytes was not improved by
420 the addition of salt (**Fig. 4D**). This may be because of the inefficient mass transfer of big molecules
421 across the liquid-gas interface into the bubble lumens (dominated by diffusion) as well as
422 competition with small molecules (solvents, other analytes). Thus, the efficiency of mass transfer
423 across the liquid-gas interface—rather than chemical similarity (polarity)—may be a more
424 important factor determining extraction rates. Although the low-molecular-weight analytes are
425 highly polar, they more readily "escape" the "crowded" liquid-phase environment (in favor of the
426 "dilute" gas-phase (bubble) environment) than the higher-molecular-weight analytes.
427 Following exposure of the newly formed bubbles to the sample matrix, the rising bubbles reach
428 the surface of liquid-headspace interface. In the case of jet drops, few (< 10) big droplets are
429 formed when the bubble internal cavity collapses (*Resch, Darrozes & Afeti, 1986*). However, in
430 the case of film drops, high numbers (*e.g.* hundreds, depending on the bubble size) of tiny droplets
431 are produced when the disintegration of the bubble film cap takes place near the liquid-gas
432 interface (*Resch, Darrozes & Afeti, 1986*). It is worth noting that—according to the previous tests
433 (*Chang & Urban, 2016*)—no liquid droplets (which might come from stirred sample and numerous
434 bubbles from effervescence) enter the detection system. This implies that all the solvent molecules

435 within the droplets evaporate before they reach the detector. Therefore, only gas-phase molecules
436 are ionized and detected by APCI-MS.
437   The FE technique involves pressurization of carrier gas in the sample chamber, which leads to
438 pressure increase in the headspace. The released gas-phase molecules are directed to the detector
439 due to the pressure difference between the sample chamber headspace and detection system.
440 Increasing extract transfer tubing length (**Fig. 2B**), and emulating slow decompression by pulsing
441 V2 at a low duty cycle (**Fig. S3**), reveals the influence of gas flow rate on FE performance. Low
442 flow rate of the gaseous extract extends FE duration and increases the exposure of bubbles to the
443 liquid matrix. The temporal profiles of the carbon dioxide flow rate showed that the gas flow rate
444 increases abruptly when depressurization occurs (V2 open), then it drastically decreases within ~
445 0.7 s after opening V2 (**Fig. S8**). On turning on the carrier gas supply (V1 open), the gas flow rate
446 again slightly increases, and finally stabilizes (~ 1.2 s after opening V1). Interestingly, the temporal
447 profile of the initial gas flow rate bears a resemblance to the temporal profiles of the ion currents
448 of some analytes (*e.g.* EPE, EHP; **Fig. S8** and **S5**, 2 s). It must be pointed out that APCI-MS is a
449 mass-sensitive detector, and the ion signal is proportional to the absolute amount of the analyte
450 molecule entering the detection system in a time unit (sample introduction rate) (*Urban, 2016*;
451 *Prabhu, Witek & Urban, 2019*). Additionally, a sudden release of considerable amount of gaseous
452 effluents into the ion chamber may lead to a transient carryover effect within the ion source.
453 Extended residence of the large amount of gaseous extract in the ion source can lead to peak tailing.
454 Interestingly, different compounds reveal distinct temporal profiles, and their signals reach
455 maxima at different time points (**Fig. S5**). This may be because the VOCs with various diffusivities
456 are stratified in the headspace, or the fact that it takes more time to extract less volatile compounds
457 (*e.g.* EN) by the emerging bubbles (**Fig. 7**). Nevertheless, with the aid of carrier gas flow (V1
458 open), larger molecules eventually arrive in the detection system following a short delay (~ 12 s
459 after opening V2).
460

Conclusions

462 We have characterized FE process taking into account various factors related to the instrument,
463 method, sample, and analytes. Some of the tested factors (*e.g.* diameter and length of the extract
464 transfer tubing, alcohol concentrations, presence of salt) have a significant effect on the extraction
465 performance, while others (*e.g.* gas type, presence of surfactants and nucleation sites) do not affect
466 it to a great extent. This information provides the basis for boosting extraction efficiency to detect
467 low-abundance analytes. It can also help analysts to predict the occurrence of matrix effects when
468 analyzing real samples. It is proposed that volatile analytes are extracted into bubble lumens. Small
469 molecules more readily diffuse into the bubble lumens, while the diffusion of bigger molecules
470 takes more time. Thus, the analytes with different molecular weights reveal distinct temporal
471 profiles, and are detected at different times. The high amplitudes of the MS signals corresponding
472 to small molecules are attributed to high extraction yields of such species as well as the
473 characteristics of the APCI-MS detection system, which is vulnerable to changes in sample flow
474 rate. Overall, the results delimit the applicability of the FE technique, thus allowing one to predict

475 in which cases the technique can be used, and point out which parameters need to be optimized
476 during FE-based method development.
477

Acknowledgements

479 We thank Prof. Chien-Ming Tseng for his help.

480

References

482 **Abeel SM, Vickers AK, Decker D. 1994.** Trends in purge and trap. *Journal of*
483 *Chromatographic Science* **32**:328-338 DOI: 10.1093/chromsci/32.8.328.
484 **Alexovič M, Dotsikas Y, Bober P, Sabo J. 2018.** Achievements in robotic automation of
485 solvent extraction and related approaches for bioanalysis of pharmaceuticals. *Journal of*
486 *Chromatography B* **1092**:402-421 DOI: 10.1016/j.jchromb.2018.06.037.
487 **Cao C, Zhang L, Zhang X-X, Du F-P. 2013.** Effect of gum arabic on the surface tension and
488 surface dilational rheology of trisiloxane surfactant. *Food Hydrocolloids* **30**:456-462 DOI:
489 10.1016/j.foodhyd.2012.07.006.
490 **Chang C-H, Urban PL. 2016.** Fizzy extraction of volatile and semivolatile compounds into the
491 gas phase. *Analytical Chemistry* **88**:8735-8740 DOI: 10.1021/acs.analchem.6b02074.
492 **Chaudhari RV, Hofmann H. 1994.** Coalescence of gas bubbles in liquids. *Reviews in Chemical*
493 *Enginnering* **10**:131-190 DOI: 10.1515/REVCE.1994.10.2.131.
494 **Chingin K, Cai Y, Liang J, Chen H. 2016.** Simultaneous preconcentration and desalting of
495 organic solutes in aqueous solutions by bubble bursting. *Analytical Chemistry* **88**:5033-5036
496 DOI: https://doi.org/10.1021/acs.analchem.6b00582.
497 **Chingin K, Yan R, Zhong D, Chen H. 2018.** Enrichment of Surface-Active Compounds in
498 Bursting Bubble Aerosols. *ACS Omega* **3**:8709-8717 DOI: 10.1021/acsomega.8b01157.
499 **Coelho PM, Pinho C. 2007.** Considerations about equations for steady state flow in natural gas
500 pipelines. *Journal of the Brazilian Society of Mechanical Sciences and Engineering* **29**:262-273
501 DOI: 10.1590/S1678-58782007000300005.
502 **Dean RB. 1944.** The formation of bubbles. *Journal of Applied Physics* **15**:446-451 DOI:
503 10.1063/1.1707453.
504 **Fang C-K, Ko H-C, Yang C-W, Lu Y-H., Hwang I-S. 2016.** *Scientific Reports* **6**:24651 DOI:
505 10.1038/srep24651.
506 **Gevantman LH. 2000.** Solubility of selected gases in water. *Nitric Oxide* **308**:8-80－8-83.
507 **Hanafizadeh P, Eshraghi J, Kosari E, Ahmed WH. 2015.** The effect of gas properties on
508 bubble formation, growth, and detachment. *Particulate Science and Technology* **33**:645-651
509 DOI: 10.1080/02726351.2015.1017033.
510 **Harris JM. 2013.** *Poly(ethylene glycol) Chemistry: Biotechnical and Biomedical Applications*,
511 1st ed.; Springer Science & Business Media, New York.
512 **Hawthorne SB. 1990.** Analytical-scale supercritical fluid extraction. *Analytical Chemistry* **62**:
513 633A-642A DOI: 10.1021/ac00210a001.

514 **Hildebrand SH, Carey JA. 1969.** *Improved Method of and Means for Dispensing Carbonated*
515 *Liquids from Containers*. UK Patent No. 1266351.
516 **Hyde AM, Zultanski SL, Waldman JH, Zhong YL, Shevlin M, Peng F. 2017.** General
517 principles and strategies for salting-out informed by the Hofmeister series. *Organic Process*
518 *Research & Development* **21**:1355-1370 DOI: 10.1021/acs.oprd.7b00197.
519 **Jones SF, Evans GM, Galvin KP. 1999.** Bubble nucleation from gas cavities—a review.
520 *Advances in Colloid and Interface Science* **80**:27-50 DOI: 10.1016/S0001-8686(98)00074-8.
521 **Lee WT, Devereux MG. 2011.** Foaming in stout beers. *American Journal of Physics* **79**:991-
522 998 DOI: 10.1119/1.3620416.
523 **Liger-Belair G. 2005.** The physics and chemistry behind the bubbling properties of champagne
524 and sparkling wines: a state-of-the-art review. *Journal of Agricultural and Food Chemistry*
525 **53**:2788-2802 DOI: 10.1021/jf048259e.
526 **Liger-Belair G, Voisin C, Jeandet P. 2005.** Modeling nonclassical heterogeneous bubble
527 nucleation from cellulose fibers: application to bubbling in carbonated beverages. *The Journal of*
528 *Physical Chemistry B* **109**:14573-14580 DOI: 10.1021/jp051650y.
529 **Liger-Belair G, Polidori G, Jeandet, P. 2008.** Recent advances in the science of champagne
530 bubbles. *Chemical Society Reviews* **37**:2490-2511 DOI: 10.1039/B717798B.
531 **Liger-Belair G. 2012.** The physics behind the fizz in champagne and sparkling wines. *The*
532 *European Physical Journal Special Topics* **201**:1-88 DOI: 10.1140/epjst/e2012-01528-0.
533 **Lubetkin SD. 2003.** Why is it much easier to nucleate gas bubbles than theory predicts?
534 *Langmuir* **19**: 2575-2587 DOI: 10.1021/la0266381.
535 **Mason EA, Kronstadt B. 1967.** Graham's laws of diffusion and effusion. *Journal of Chemical*
536 *Education* **44**:740-744 DOI: 10.1021/ed044p740.
537 **Moroi Y, Motomura K, Matuura R. 1974.** The critical micelle concentration of sodium
538 dodecyl sulfate-bivalent metal dodecyl sulfate mixtures in aqueous solutions. *Journal of Colloid*
539 *and Interface Science* **46**:111-117 DOI: 10.1016/0021-9797(74)90030-7.
540 **Pelipenko J, Kristl J, Rošic R, Baumgartner S, Kocbek P. 2012.** Interfacial rheology: an
541 overview of measuring techniques and its role in dispersions and electrospinning. *Acta*
542 *Pharmaceutica* **62**:123-140 DOI: 10.2478/v10007-012-0018-x.
543 **Poole CF. 2020.** Chapter 1 - milestones in the development of liquid-phase extraction
544 techniques. *Liquid-Phase Extraction* 1-44 DOI: 10.1016/B978-0-12-816911-7.00001-3.
545 **Prabhu GRD, Urban PL. 2017.** The dawn of unmanned analytical laboratories. *TrAC Trends in*
546 *Analytical Chemistry* **88**:41-52 DOI: 10.1016/j.trac.2016.12.011.
547 **Prabhu GRD, Witek HA, Urban PL. 2019.** Programmable flow rate scanner for evaluating
548 detector sensitivity regime. *Sensors and Actuators B: Chemical* **282**:992-998 DOI:
549 10.1016/j.snb.2018.11.033.
550 **Rajib MM, Farzeen P, Ali M. 2017.** Study on the number density of nanobubbles at varying
551 concentration of ethanol in ethanol-water solution. *AIP Conference Proceedings* **1919**:020018-1
552 －020018-7 DOI: 10.1063/1.5018536.
553 **Rathakrishnan, E. 2004.** *Gas Tables*. Revised Ed., Universities Press: India.

554 **Resch FJ, Darrozes JS, Afeti GM. 1986.** Marine liquid aerosol production from bursting of air
555 bubbles. *Journal of Geophysical Research: Oceans* **91**:1019-1029 DOI:
556 10.1029/JC091iC01p01019.

557 **Sandoval-Robles JG, Delmas H, Couderc JP. 1981.** Influence of turbulence on mass transfer
558 between a liquid and a solid sphere. *AIChE Journal* **27**:819-823 DOI: 10.1002/aic.690270516.

559 **Setschenow J. 1889.** Über die konstitution der salzlösungen auf grund ihres verhaltens zu
560 kohlensäure. *Zeitschrift für Physikalische Chemie* **4**:117-125 DOI: 10.1515/zpch-1889-0409.

561 **Shimoda M, Ishikawa H, Kawano T, Osajima Y. 1994.** Extraction of volatile compounds from
562 aqueous solution using micro bubble, gaseous, supercritical and liquid carbon dioxide. *Journal of*
563 *Food Science* **59**:231-232 DOI: 10.1111/j.1365-2621.1994.tb06937.x.

564 **Stokes GG. 1851.** On the effect of the internal friction of fluids on the motion of pendulums.
565 *Transactions of the Cambridge Philosophical Society* **9**:8-93 DOI:
566 10.1017/cbo9780511702266.002.

567 **Takagi S, Matsumoto Y. 2011.** Surfactant effects on bubble motion and bubbly flows. *Annual*
568 *Review of Fluid Mechanics* **43**:615-636 DOI: 10.1146/annurev-fluid-122109-160756.

569 **Thomas AS, Elcock AH. 2007.** Molecular dynamics simulations of hydrophobic associations in
570 aqueous salt solutions indicate a connection between water hydrogen bonding and the
571 Hofmeister effect. *Journal of the American Chemical Society* **129**:14887-14898 DOI:
572 10.1021/ja073097z.

573 **Urban PL. 2016.** Clarifying misconceptions about mass and concentration sensitivity. *Journal of*
574 *Chemical Education* **93**:984-987 DOI: 10.1021/acs.jchemed.5b00986.

575 **Urban PL. 2018.** Prototyping instruments for the chemical laboratory using inexpensive
576 electronic modules. *Angewandte Chemie International Edition* **57**:11074-11077 DOI:
577 10.1002/anie.201803878.

578 **Wang T, Lenahan R. 1984.** Determination of volatile halocarbons in water by purge-closed
579 loop gas chromatography. *Bulletin of Environmental Contamination and Toxicology* **32**:429-438
580 DOI: 10.1007/BF01607519.

581 **Wyasu G, Okereke NZ-J. 2012.** Improving the film forming ability of gum Arabic. *Journal of*
582 *Natural Product and Plant Resources* **2**:314-317.

583 **Yang H-C, Chang C-H, Urban PL. 2017.** Fizzy extraction of volatile organic compounds
584 combined with atmospheric pressure chemical ionization quadrupole mass spectrometry. *Journal*
585 *of Visualized Experiments* **125**:e56008 DOI: 10.3791/56008.

586 **Yang H-C, Urban PL. 2019.** On-line coupling of fizzy extraction with gas chromatography
587 *Analytical and Bioanalytical Chemistry* **411**:2511-2520 DOI: 10.1007/s00216-019-01755-9.

588 **Yang H-C, Chang C-M, Urban PL. 2019.** *Heliyon* **5**:e01639 DOI:
589 10.1016/j.heliyon.2019.e01639.

590 **Zheng N. 2020.** 21 - Automated and high-throughput extraction approaches. *Solid-Phase*
591 *Extraction* 573-588 DOI: 10.1016/B978-0-12-816906-3.00021-2.

592 **Zimmerman WB, Tesar V, Butler S, Bandulasena HC. 2008.** Microbubble generation. *Recent*
593 *Patents on Engineering* **2**:1-8 DOI: 10.2174/187221208783478598.

Figure 1

Simplified scheme of the experimental setup used to conduct FE in conjunction with APCI-MS.

Chemistry Journals
Analytical, Inorganic, Organic, Physical, Materials Science
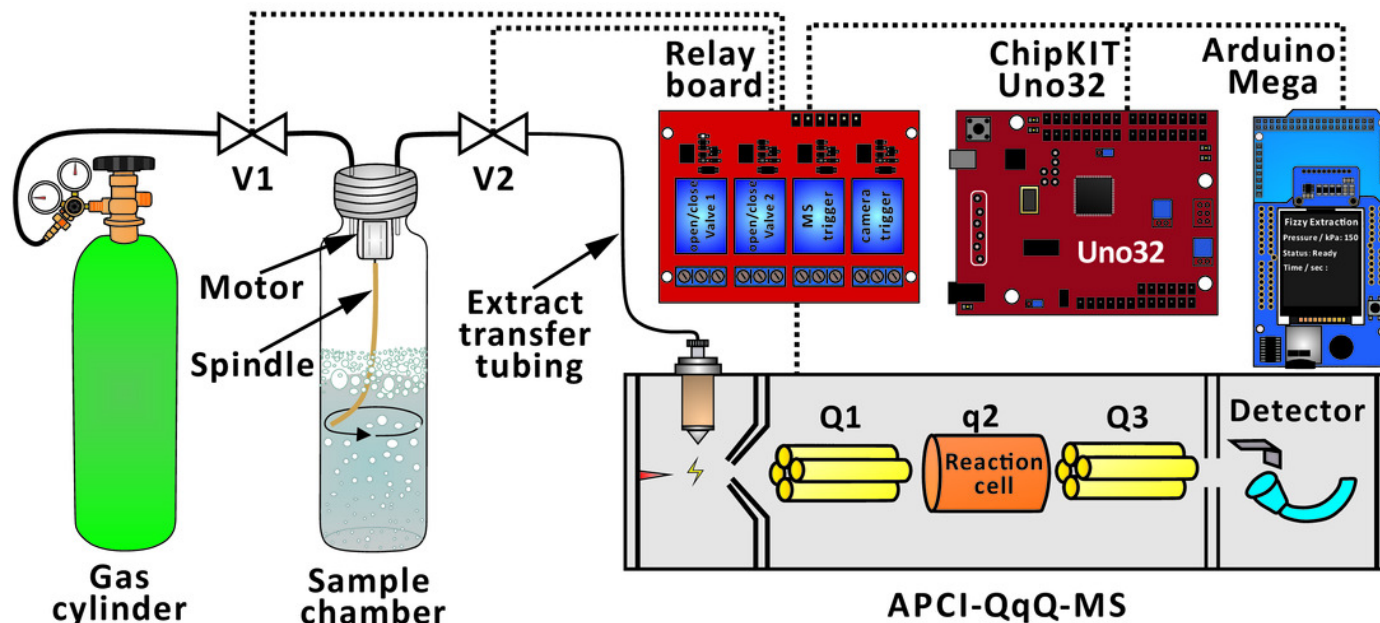
Figure 2

Influence of instrument-related factors on EF and *S/N*: (A) extract transfer tubing diameter; (B) extract transfer tubing length. Error bars represent standard deviation (*n* = 3).
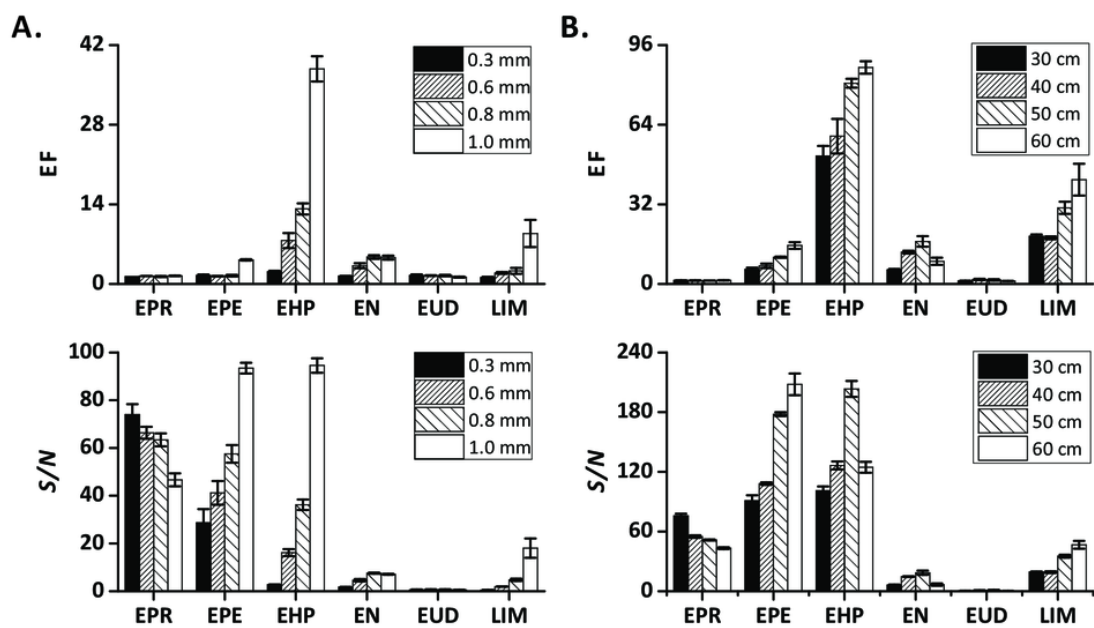
Figure 3

Influence of method-related factors on EF and *S/N*:

(A) carrier gas type; (B,C) fast decompression (no pulse was applied) *vs.* slow decompression (a relay was used to open (o) and close (c) V2 continuously with different "open" duty cycles to provide pulsations; cycle duration, 400 ms; (B) pulsing only in *stage 1* of the extraction step; (C) pulsing in both stages of the extraction step). (D) extraction time in *stage 1* of the extraction step (total extraction time, 30 s). Error bars represent standard deviation (*n* = 3).

PeerJ **Chemistry Journals**

Analytical, Inorganic, Organic, Physical, Materials Science
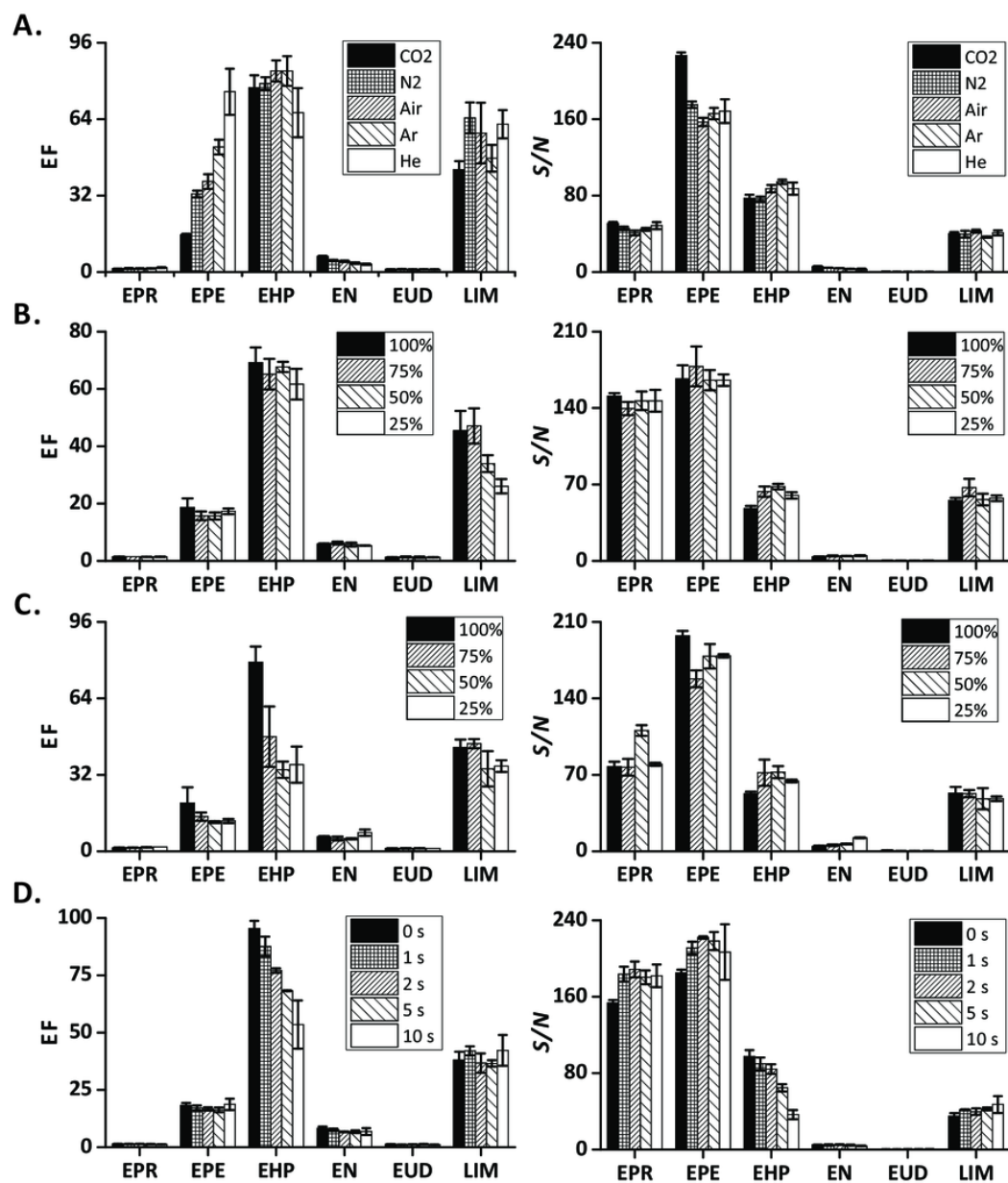
Figure 4

Influence of sample-related factors (additives in the sample matrix) on EF and *S/N*:

(A) methanol; (B) ethanol; (C) isopropanol; (D) sodium chloride; (E) gum arabic; (F) SDS; (G) PEG 400; (H) cotton fibers. In (A-C, and G) the units are vol. %; in (D and E) the units are wt. %. Error bars represent standard deviation (*n* = 3).
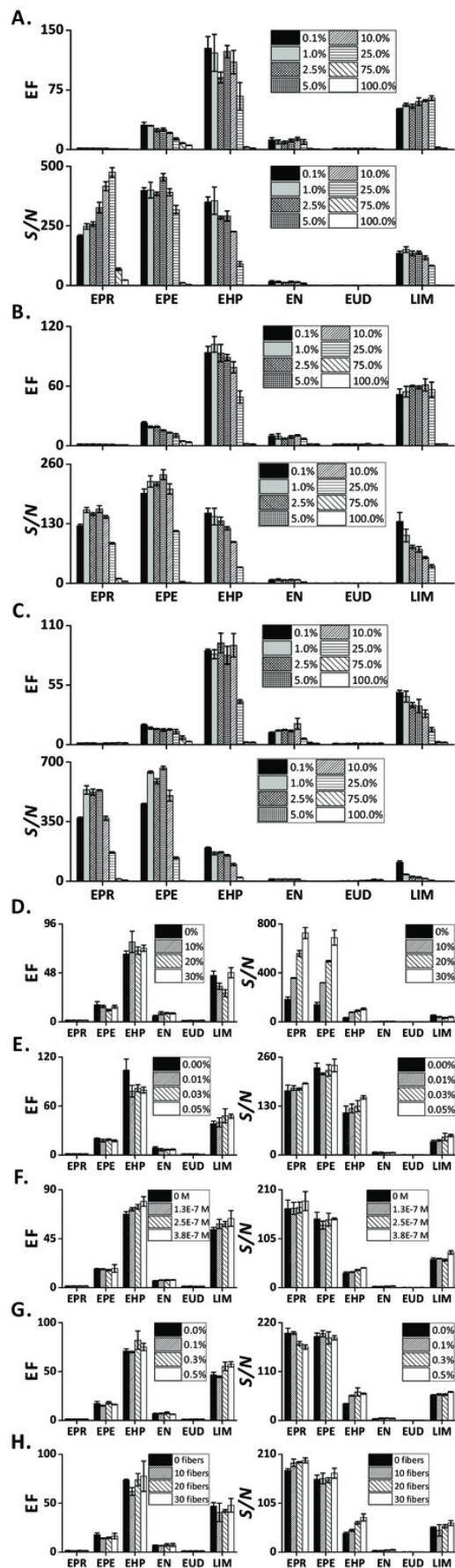
Figure 5

Influence of analyte-related factors on EF, *S/N* and $S_{corrected}$:

(A) carbon number; (B) boiling point; (C) logarithm of octanol-water partition coefficient; (D) surface tension; (E) vapor pressure; (F) solubility in water. Error bars represent standard deviation (*n* = 3).
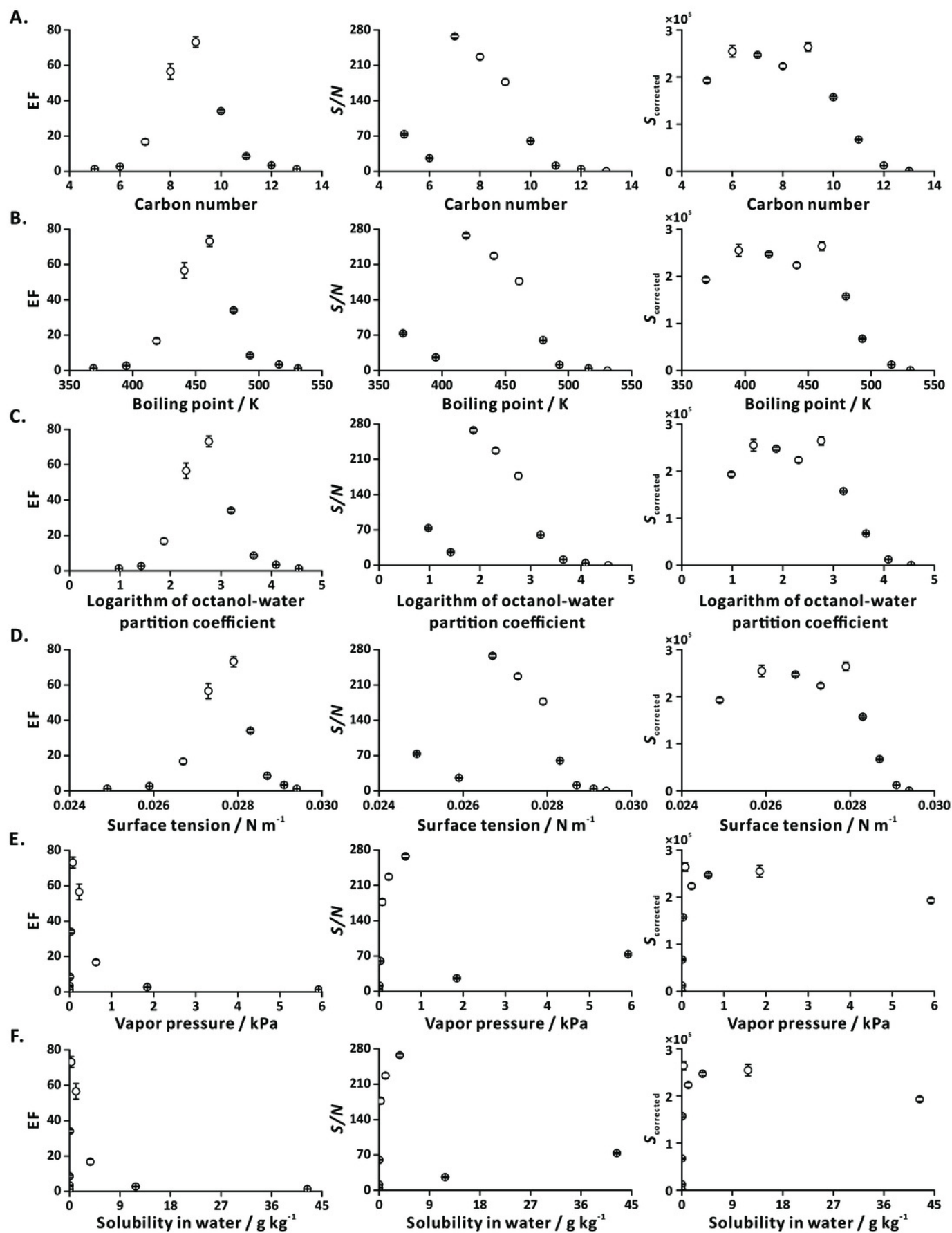
Figure 6

Hypothetical pathways of analyte transfer from liquid to gas phase in FE.

 Chemistry Journals
Analytical, Inorganic, Organic, Physical, Materials Science
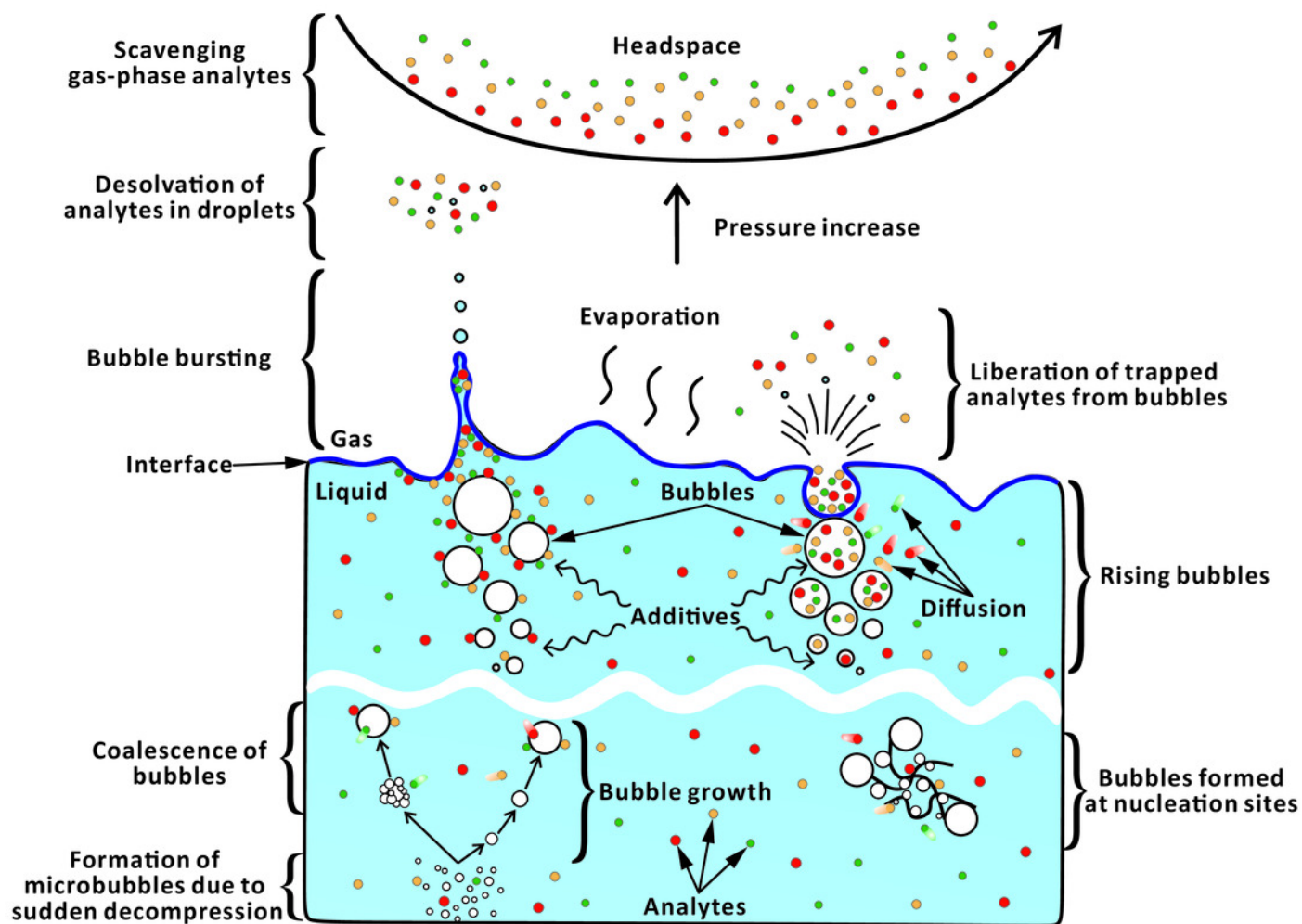
Figure 7

Extraction analyte flux as a function of time in the extraction step, defined here as the ratio of extracted ion current (EIC) and momentary carrier gas flow rate (FR).

Solid line represents EPE; dashed line represents EHP; dotted line represents EN. Here, time 0 s corresponds to the start of the extraction step (*stage 1*). The averaged analyte fluxes obtained in three replicate experiments are displayed.